

Article

Synthesis and X-ray Crystal Structure Analysis of Substituted 1,2,4-Triazolo [4',3':2,3]pyridazino[4,5-*b*]indole and Its Precursor

Ahmed T. A. Boraei ^{1,*}, Elsayed H. Eltamany ¹, Matti Haukka ² , Saied M. Soliman ³, Assem Barakat ^{4,*}  and Manar Sopaih ¹

¹ Chemistry Department, Faculty of Science, Suez Canal University, Ismailia 41522, Egypt; elsayed_mostafa@science.edu.eg or s.eltamany51@yahoo.com (E.H.E.); manar_shalabi@science.edu.eg (M.S.)

² Department of Chemistry, University of Jyväskylä, P.O. Box 35, FI-40014 Jyväskylä, Finland; matti.o.haukka@jyu.fi

³ Chemistry Department, Faculty of Science, Alexandria University, P.O. Box 426, Alexandria 21321, Egypt; saeed.soliman@alexu.edu.eg

⁴ Department of Chemistry, College of Science, King Saud University, P.O. Box 2455, Riyadh 11451, Saudi Arabia

* Correspondence: ahmed_boraei@science.suez.edu.eg or ahmed_tawfeek83@yahoo.com (A.T.A.B.); ambarakat@ksu.edu.sa (A.B.); Tel.: +966-11467-5901 (A.B.); Fax: +966-11467-5992 (A.B.)

Abstract: The hit compound 1,2,4-triazolo[4',3':2,3]pyridazino[4,5-*b*]indole **3** was synthesized from the reflux of 4-amino-5-indolyl-1,2,4-triazole-3-thione **1** with 4'-bromoacetophenone **2** in methanol catalyzed by concentrated HCl and the desired final molecule was obtained by recrystallization from methanol. The suggested structures of compounds **1** and **3** based on the spectral characterizations were confirmed by X-ray single crystal diffraction analysis. Compound **3** crystallized in the triclinic crystal system and *P*-1 space group with $a = 5.9308(2)$ Å, $b = 10.9695(3)$ Å, $c = 14.7966(4)$ Å, $\alpha = 100.5010(10)^\circ$, $\beta = 98.6180(10)^\circ$, and $\gamma = 103.8180(10)^\circ$. On the other hand, the crystal system of **1** is monoclinic, where $a = 6.23510(10)$ Å, $b = 26.0156(4)$ Å, $c = 12.4864(2)$ Å, $\beta = 93.243(2)^\circ$ and the space group is *P*2₁. The triazole and indole rings are found twisted from each other in both compounds. The twist angle is higher in **3** (12.65°) than **1** (4.94–7.22°). In the case of the former, the H ... H (39.6%), H ... C (22.0%), N ... H (12.8%) and Br ... H (13.2%) contacts are the most dominant while the C ... C, C ... H, Br ... H, N ... H and S ... S contacts have the characteristics of strong interactions. In the latter, the C ... H, N ... H, S ... H, S ... S, and C ... C contacts are the most important. In this case, the percentages of the H ... H, C ... H, N ... H and S ... H contacts are in the range of 34.9–37.4, 20.5–24.0, 12.2–13.6, 14.0–15.8, respectively. In both systems, the shape index and curvedness of surfaces confirmed the presence of π - π stacking interactions.

Keywords: pyridazino[4,5-*b*]indol-4-one; indoles; pyridazines; X-ray single crystal; Hirshfeld surface analysis



Citation: Boraei, A.T.A.; Eltamany, E.H.; Haukka, M.; Soliman, S.M.; Barakat, A.; Sopaih, M. Synthesis and X-ray Crystal Structure Analysis of Substituted 1,2,4-Triazolo [4',3':2,3]pyridazino[4,5-*b*]indole and Its Precursor. *Crystals* **2023**, *13*, 1036. <https://doi.org/10.3390/cryst13071036>

Academic Editor: Waldemar Maniukiewicz

Received: 1 June 2023

Revised: 25 June 2023

Accepted: 26 June 2023

Published: 29 June 2023



Copyright: © 2023 by the authors. Licensee MDPI, Basel, Switzerland. This article is an open access article distributed under the terms and conditions of the Creative Commons Attribution (CC BY) license (<https://creativecommons.org/licenses/by/4.0/>).

1. Introduction

Among the poly nitrogen containing compounds, whose importance in the field of biology and smart materials is well known [1,2], it is worth mentioning the pyridazino[4,5-*b*]indol-4-ones, which are a class of heterocycles consisting of fused tricyclic rings having pyridazine and indolyl scaffolds. This conjugate has been determined to be an interesting pharmacophore in drug discovery research. In cancer treatment, in particular the pyridazino[4,5-*b*]indol-4-one as an *aza*-heterocycle class compound exhibited high efficacy against many human cancer cells and targeted PI3K α and DYRK1A5 inhibitory activity [3,4]. Many other biological features have been reported for the pyridazino[4,5-*b*]indol-4-ones as anti-microbial agents [5,6], anti-hypertensive [7,8], anti-viral (HIV-1) [9] and blood platelet aggregation inhibitors [10]. Additionally, pyridazino[4,5-*b*]indol-4-one which can be classified as β -carboline or γ -carboline core structures, showed interesting

pharmacological potencies [11] such as binding with DNA, genotoxic, mutagenic and cytotoxicity activities [12]. To design new molecules based on pyridazino[4,5-*b*]indol-4-one as a pharmacological feature is an attractive challenge.

Many representative examples reported so far derive from the pyridazino[4,5-*b*]indol-4-one carboline framework structure, such as SSR180575 (Figure 1) which is a neuroprotective agent targeted to TSPO or PBR receptors with high nanomolar binding affinity [13,14]. ZFD-10 is another representative example which was reported recently to be an anti-viral agent against ZIKV [15]. The authors claimed that this compound was able to inhibit the ZIKV NS5 RdRp receptor and confirmed this using an RNA polymerase assay [15]. Sarhan, et al., designed and evaluated a novel pyridazino[4,5-*b*]indol-4-one derivative against the human breast cancer cell (MCF-7), and was identified as a phosphoinositide 3-kinase (PI3K) inhibitor [16]. Besirli and co-workers developed a small molecule as a next generation PKM2 activator, signaling photoreceptor apoptosis [17]. Salama and co-workers have identified new molecules based on pyridazino[4,5-*b*]indol-4-one as multitargeting inhibitors binding targets including EGFR, PI3K, and AKT [18].

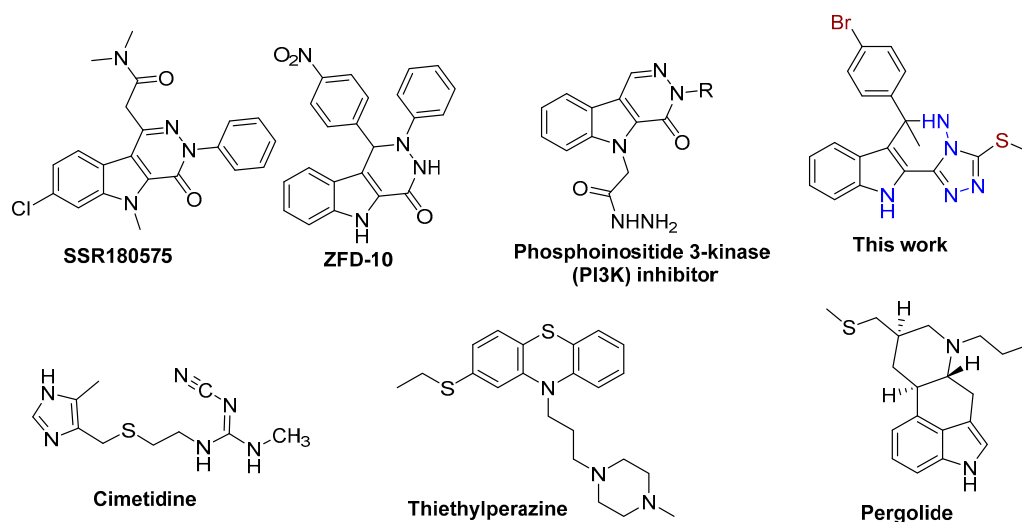


Figure 1. Some pyridazino[4,5-*b*]indol-4-one derivatives and selected thioether drugs of biological importance.

Many other biological activities have been reported to be targeted by pyridazino[4,5-*b*]indol-4-one [19–27], such as neoplastic progression, neuroinflammation, acute and chronic inflammation, congestive heart failure (CHF), antiarrhythmic, serotonin antagonists [28–30], among others. Thioether drugs represents one of the most important constituents of sulfur containing drugs. The demonstrative pharmaceutical drugs include cimetidine (mainly used for treatment of heartburn and peptic ulcers), thiethylperazine (important antagonist of dopamine receptors), and pergolide (ergoline-based dopamine receptor agonist used in some countries for the treatment of Parkinson’s disease) [31,32].

Based on these findings mentioned above and in continuation of our research program for the synthesis of novel heterocycles, we report here new pyridazino[4,5-*b*]indol-4-one derivatives. The chemical architectures were assigned based on a single crystal X-ray diffraction analysis and other spectrophotometric tools. Additionally, supramolecular insights have been explored using Hirshfeld surface analysis.

2. Materials and Methods

Melting points were determined using melting-point apparatus (SMP10) in open capillaries and are uncorrected. Chemicals, solvents and reagents were purchased from Sigma-Merck (Burlington, MA, USA) and Alfa Aesar (Stoughton, MA, USA). The reaction progress and product purity was observed by thin layer chromatography (TLC) pre-coated plates with silica gel 60 F₂₅₄ with a thickness of 0.25 mm (Merck). Nuclear magnetic reso-

nance (^1H NMR and ^{13}C NMR) spectra were determined in $\text{DMSO-}d_6$ and were recorded on Bruker AC 400 MHz spectrometers (Billerica, MA, USA) using TMS as an internal reference standard. δ (ppm) was used for chemical shift description and values of coupling constants were given in Hz. CHNS-microanalysis was performed on a Flash EA-1112 instrument (Thermo Fisher Scientific, San Diego, CA, USA).

4-Amino-5-(1*H*-indol-2-yl)-2,4-dihydro-3*H*-1,2,4-triazole-3-thione **1** Synthetic procedures followed [33].

Yield: 78%, m.p. 288–289 °C [Lit. [31] 293–294 °C]. ^1H NMR (400 MHz, $\text{DMSO-}d_6$) δ 14.01 (s, 1H), 11.77 (s, 1H), 7.67 (d, $J = 7.8$ Hz, 1H), 7.55–7.47 (m, 2H), 7.22 (t, $J = 7.4$ Hz, 1H), 7.07 (t, $J = 7.4$ Hz, 1H), 5.97 (s, 2H); ^{13}C NMR (101 MHz, $\text{DMSO-}d_6$) δ 167.08, 144.93, 137.22, 127.74, 123.99, 123.28, 121.65, 120.37, 112.47, 105.25; Elemental Analysis Calc. for $[\text{C}_{10}\text{H}_9\text{N}_5\text{S}]$: C, 51.93; H, 3.92; N, 30.28; S, 13.86 found C, 51.99; H, 3.82; N, 30.21; S, 14.01.

6-(4-Bromophenyl)-6-methyl-3-(methylthio)-6,11-dihydro-5*H*-[1,2,4]triazolo [4',3':2,3]p- yridazino[4,5-*b*]indole **3**

To a mixture of **1** (2.0 mmol) and 4'-Bromoacetophenone **2** (2.1 mmol) in 10 mL MeOH, conc. HCl (0.3 mL) was added, and the mixture was refluxed for 6 h, then cooled. The ppt was collected by filtration, dried and recrystallized from MeOH.

Yield: 65%, m.p. 305–306 °C. ^1H NMR (400 MHz, $\text{DMSO-}d_6$) δ 12.43 (s, 1H), 7.82 (d, $J = 7.7$ Hz, 1H), 7.54 (d, $J = 7.8$ Hz, 1H), 7.43 (d, $J = 7.7$ Hz, 2H), 7.28 (d, $J = 7.5$ Hz, 3H), 7.19 (d, $J = 10.9$ Hz, 2H), 2.66 (s, 3H), 2.01 (s, 3H); ^{13}C NMR (101 MHz, $\text{DMSO-}d_6$) δ 150.20, 146.44, 144.95, 137.89, 131.57, 128.46, 125.23, 123.80, 121.41, 121.19, 120.97, 120.50, 117.58, 113.11, 61.88, 27.27, 13.76; Elemental Analysis Calc. for $[\text{C}_{19}\text{H}_{16}\text{BrN}_5\text{S}]$: C, 53.53; H, 3.78; Br, 18.74; N, 16.43; S, 7.52 found C, 53.73; H, 3.95; Br, 18.89; N, 16.39; S, 7.63.

2.1. X-ray Structure Determinations

The crystals of **1** and **3** were immersed in cryo-oil, mounted on a loop, and measured at a temperature of 120 K and 170 K, respectively. The X-ray diffraction data were collected on a Bruker Kappa Apex II (**3**) or a Rigaku Oxford Diffraction Supernova (**1**) diffractometer using Mo $K\alpha$ radiation. The Denzo-Scalepack [34] (**3**) or CrysAlisPro [35] (**1**) software packages were used for cell refinements and data reductions. The structures were solved by the intrinsic phasing method using the SHELXT [36] software. A numerical (**3**) absorption correction (SADABS [37]) or Gaussian (**1**) absorption correction (CrysAlisPro [33]) was applied to the intensities before the structure solution. Structural refinements were carried out using SHELXL [38] software with the SHELXLE [39] graphical user interface. The crystal of **1** was solved in the chiral space group $P2_1$ and the asymmetric unit contained four crystallographically independent molecules. The NH and NH_2 hydrogen atoms were located from the difference Fourier map and refined isotopically. All other hydrogen atoms were positioned geometrically and constrained to ride on their parent atoms, with $\text{C-H} = 0.95 - 0.98$ Å and $U_{\text{iso}} = 1.2 - 1.5 \cdot U_{\text{eq}}(\text{parent atom})$. The crystallographic details are summarized in Table 1.

Table 1. Crystal Data.

	3	1
CCDC no.	2266558	2266559
empirical formula	$\text{C}_{19}\text{H}_{16}\text{BrN}_5\text{S}$	$\text{C}_{10}\text{H}_9\text{N}_5\text{S}$
fw	426.34	231.28
temp (K)	170(2) K	120(2)
λ (Å)	0.71073 Å	0.71073
crystal system	Triclinic	Monoclinic
space group	$P 1$	$P2_1$

Table 1. Cont.

	3	1
<i>a</i> (Å)	5.9308(2)	6.23510(10)
<i>b</i> (Å)	10.9695(3)	26.0156(4)
<i>c</i> (Å)	14.7966(4)	12.4864(2)
α (deg)	100.5010(10)	90
β (deg)	98.6180(10)	93.243(2)
γ (deg)	103.8180(10)	90
<i>V</i> (Å ³)	900.07(5)	2022.17(6)
<i>Z</i>	2	8
ρ_{calc} (Mg/m ³)	1.573	1.519
μ (Mo K α) (mm ⁻¹)	2.413	0.297
No. reflections.	19858	13486
Completeness to theta = 25.242°	99.1%	99.9%
Unique reflns.	5240	13486
GOOF (<i>F</i> ²)	1.043	1.028
<i>R</i> _{int}	0.0278	0.0376
<i>R</i> ₁ ^a (<i>I</i> ≥ 2 σ)	0.0433	0.0425
<i>wR</i> ₂ ^b (<i>I</i> ≥ 2 σ)	0.0913	0.0995

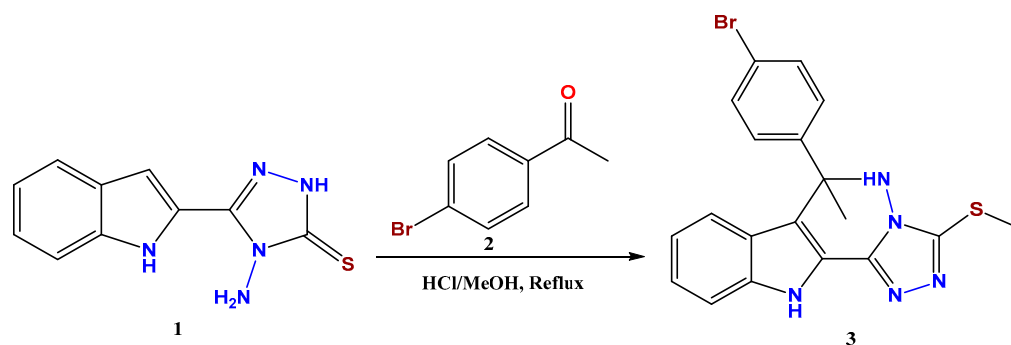
^a $R_1 = \sum ||F_o| - |F_c|| / \sum |F_o|$. ^b $wR_2 = [\sum [w(F_o^2 - F_c^2)^2] / \sum [w(F_o^2)^2]]^{1/2}$.

2.2. Hirshfeld Surface Analysis

The topology analyses were performed using the Crystal Explorer 17.5 program [40].

3. Results and Discussion

The starting precursor 4-amino-5-(1*H*-indol-2-yl)-2,4-dihydro-3*H*-1,2,4-triazole-3-thione **1** was synthesized following the procedures outlined previously [33]. Reaction of **1** with 4'-bromoacetophenone **2** in methanol and the presence of concentrated HCl as an acid catalyst afforded 1,2,4-triazolo [4',3':2,3]pyridazino[4,5-*b*]indole **3** in good yield (Scheme 1).

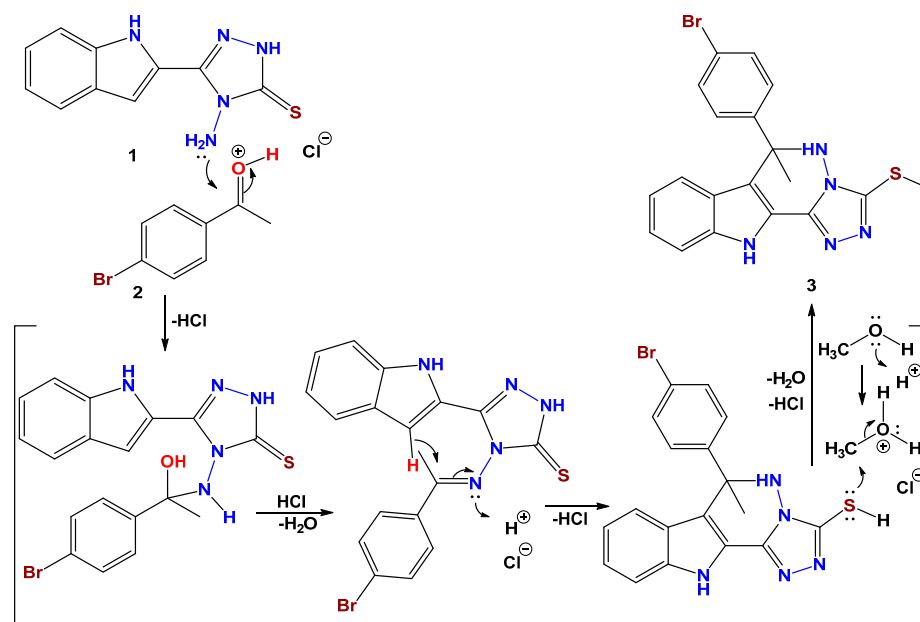


Scheme 1. Synthesis of 1,2,4-Triazolo [4',3':2,3]pyridazino[4,5-*b*]indole **3**.

The NMR supported the structure (see Figures S1–S4; Supplementary Materials) via the following signals: ¹H NMR displayed the triazole NH at 14.01 ppm, the indole NH at 11.77 ppm and the amino group protons at 5.97 ppm. In addition, ¹³C NMR detected the thiocarbonyl carbon at 167.08 ppm and the remaining triazole carbon at 144.93 ppm. The ¹H NMR of **3** displayed a signal at 12.43 ppm for indole NH, and two signals at 2.66 and 2.01 ppm for two methyl groups. Moreover, ¹³C NMR displayed the two triazole carbons at 150.20 and 146.44 ppm. The quaternary carbon was detected at 61.88 ppm. While the two methyl carbons were found at 27.27 and 13.76 ppm.

The reaction product **3** is suggested to form through the mechanism described in Scheme 2. The mechanism illustrates the role of the acid catalyst in the condensation reaction and removal of a water molecule. Secondly the mechanism also explains the role of the acid in the formation of an electrophile (the expected methyl carbocation) from

methanol as a methylating agent which then attacked from the nucleophilic sulfur atom (Scheme 2).



Scheme 2. Plausible mechanism for the synthesis of compound 3.

3.1. Crystal Structure Description

The structure of 3 is further confirmed using X-ray diffraction of a single crystal. The structure of the asymmetric unit is shown in Figure 2. As seen in this figure, there is one molecule of 3 as an asymmetric formula while four molecules are present in the unit cell. Compound 3 crystallized in the triclinic crystal system and *P*-1 space group. The unit cell parameters are $a = 5.9308(2) \text{ \AA}$, $b = 10.9695(3) \text{ \AA}$, $c = 14.7966(4) \text{ \AA}$, $\alpha = 100.5010(10)^\circ$, $\beta = 98.6180(10)^\circ$, and $\gamma = 103.8180(10)^\circ$, while $V = 900.07(5) \text{ \AA}^3$ and density is calculated to be 1.573 mg/m^3 (Table 1). The experimental geometric parameters are depicted in Table 2. The triazole and indole rings are perfectly planar but both rings are twisted from each other by 12.65° . In addition, the phenyl ring is nearly perpendicular to the mean plane of the triazole and indole moieties. The corresponding twist angles are 83.71 and 86.57° , respectively.

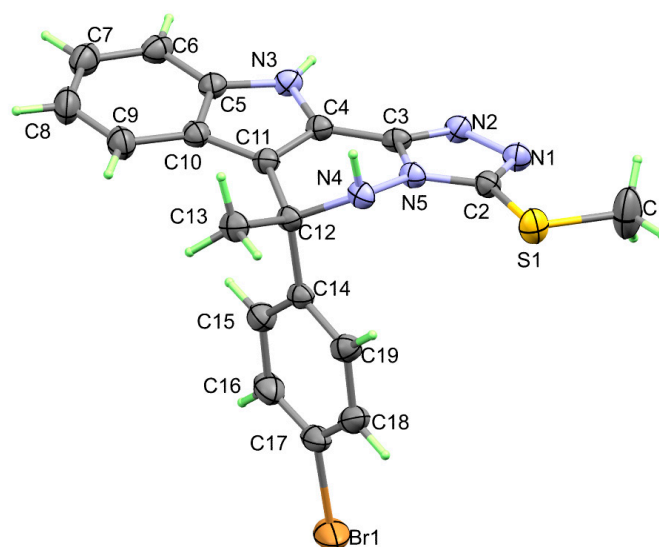


Figure 2. X-ray structure of 3.

Table 2. Bond lengths (Å) and angles (°) of **3**.

Bond	Length/Å	Bond	Length/Å
Br(1)-C(17)	1.901(2)	N(3)-C(4)	1.364(2)
S(1)-C(2)	1.729(2)	N(3)-C(5)	1.370(3)
S(1)-C(1)	1.800(3)	N(4)-N(5)	1.415(2)
N(1)-C(2)	1.319(2)	N(4)-C(12)	1.496(3)
N(1)-N(2)	1.405(2)	N(5)-C(2)	1.360(3)
N(2)-C(3)	1.314(2)	N(5)-C(3)	1.376(2)
Bond	Angle/°	Bond	Angle/°
C(2)-S(1)-C(1)	98.05(11)	N(2)-C(3)-N(5)	109.78(17)
C(2)-N(1)-N(2)	107.17(16)	N(2)-C(3)-C(4)	134.78(17)
C(3)-N(2)-N(1)	107.18(15)	N(5)-C(3)-C(4)	115.34(16)
C(4)-N(3)-C(5)	107.76(17)	N(3)-C(4)-C(11)	111.56(17)
N(5)-N(4)-C(12)	109.85(14)	N(3)-C(4)-C(3)	127.89(17)
C(2)-N(5)-C(3)	105.82(15)	C(11)-C(4)-C(3)	120.50(17)
C(2)-N(5)-N(4)	127.79(16)	N(3)-C(5)-C(6)	129.00(19)
C(3)-N(5)-N(4)	126.36(16)	N(3)-C(5)-C(10)	108.68(17)

The molecular units of **3** are connected to each other by C13-H13C ... N2, N4-H4 ... N1 and N3-H3 ... N2 non-covalent interactions shown in Figure 3A. Details of these intermolecular interactions are depicted in Table 3. The H13C ... N2, H4 ... N1 and H3 ... N2 have the shortest interaction distances of 2.54, 2.46(3) and 2.07(3) Å, respectively, while the C13 ... N2, N4 ... N1 and N3 ... N2 distances are 3.458(3), 3.270(2) and 2.854(2) Å, respectively. The corresponding C13-H13C ... N2, N4-H4 ... N1 and N3-H3 ... N2 angles are 155.7, 160(2) and 172(3)°, respectively. The packing scheme of the molecular units is shown in Figure 3B.

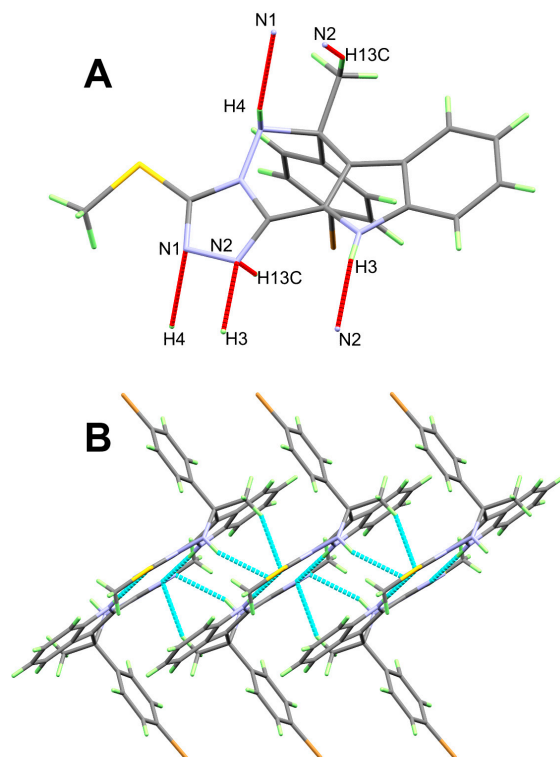
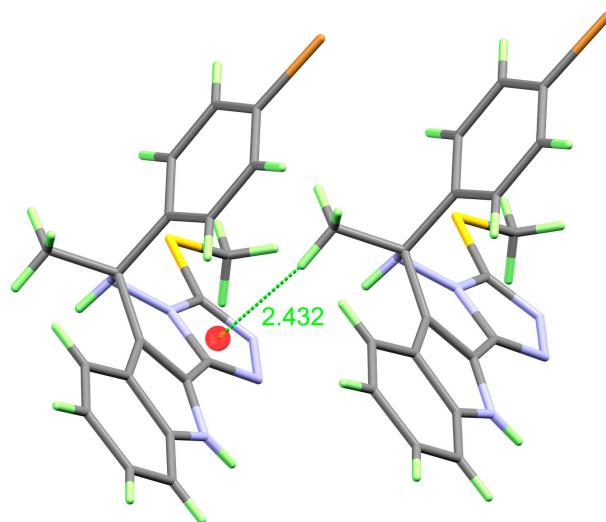
**Figure 3.** The C-H ... N/N-H ... N contacts (A) and molecular packing scheme (B) for **3**.

Table 3. Hydrogen bonds for **3** [Å and °].

D-H ... A	d(D-H)	d(H ... A)	d(D ... A)	<(DHA)	Symm. Code
N(3)-H(3) ... N(2)#1	0.79(3)	2.07(3)	2.854(2)	174(3)	#1 $-x + 1, -y + 2, -z + 1$
C(13)-H(13C) ... N(2)#2	0.98	2.54	3.458(3)	155.7	#2 $x + 1, y, z$
N(4)-H(4) ... N(1)#2	0.85(3)	2.46(3)	3.270(2)	160(2)	#2 $x + 1, y, z$

In addition, the supramolecular structure of **3** is controlled by C-H ... π interactions between the C13-H13C of the methyl group and the π -system of the triazole system. The distance between the H13C atom and the ring centroid is 2.432(3) Å. Presentation of the C-H ... π interactions is shown in Figure 4.

**Figure 4.** The C-H ... π interactions in **3**.

On the other hand, the X-ray structure of **1** is shown in Figure 5 while the detailed crystal data are given in Table 1. The crystal system of compound **1** is the more symmetric monoclinic and $P2_1$ space group. Crystal data are $a = 6.23510(10)$ Å, $b = 26.0156(4)$ Å, $c = 12.4864(2)$ Å, and $\beta = 93.243(2)^\circ$, while $V = 2022.17(6)$ Å³ and $z = 8$. The crystal density is calculated to be 1.519 mg/m³. In this crystal structure, there are four molecules of this compound that differ very little in their geometric parameters (Table 4). In this case, the twist angles between the indole and triazole rings are found to be less compared to **3**, where the twist angles are 7.22, 4.94, 6.74, and 6.21°, for molecules **A** to **D**, respectively.

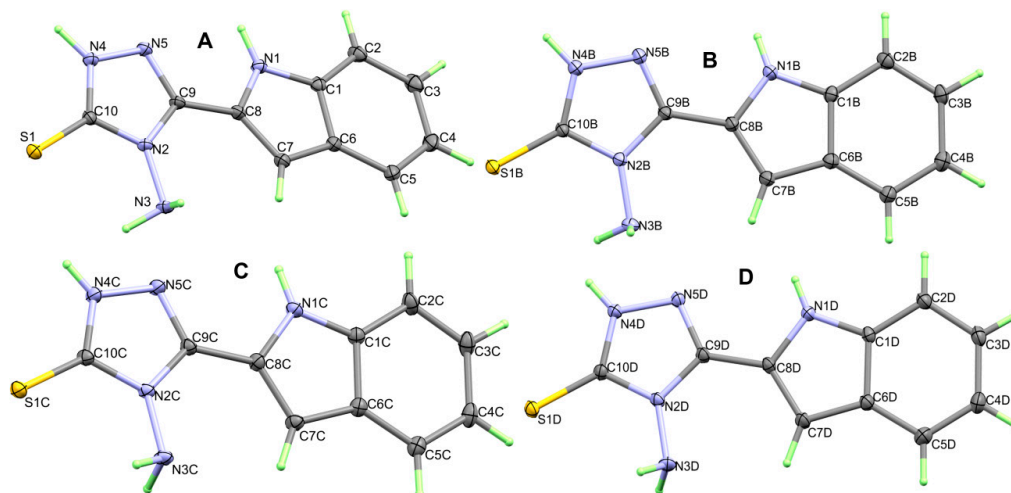
**Figure 5.** Structure of the four molecules in the asymmetric formula of **1**.

Table 4. Bond lengths (Å) and angles (°) for **1**.

Bond	Length/Å	Bond	Length/Å
S(1)-C(10)	1.675(3)	S(1C)-C(10C)	1.680(3)
N(1)-C(1)	1.378(4)	N(1C)-C(1C)	1.374(4)
N(1)-C(8)	1.382(4)	N(1C)-C(8C)	1.383(3)
N(2)-C(10)	1.370(3)	N(2C)-C(9C)	1.366(3)
N(2)-C(9)	1.371(3)	N(2C)-C(10C)	1.373(3)
N(2)-N(3)	1.407(3)	N(2C)-N(3C)	1.405(3)
N(4)-C(10)	1.343(4)	N(4C)-C(10C)	1.337(3)
N(4)-N(5)	1.373(3)	N(4C)-N(5C)	1.377(3)
N(5)-C(9)	1.316(3)	N(5C)-C(9C)	1.315(3)
S(1B)-C(10B)	1.677(3)	S(1D)-C(10D)	1.685(3)
N(1B)-C(1B)	1.376(4)	N(1D)-C(1D)	1.375(4)
N(1B)-C(8B)	1.383(4)	N(1D)-C(8D)	1.380(4)
N(2B)-C(10B)	1.378(3)	N(2D)-C(10D)	1.362(4)
N(2B)-C(9B)	1.379(3)	N(2D)-C(9D)	1.368(3)
N(2B)-N(3B)	1.400(3)	N(2D)-N(3D)	1.407(3)
N(4B)-C(10B)	1.336(4)	N(4D)-C(10D)	1.335(4)
N(4B)-N(5B)	1.379(3)	N(4D)-N(5D)	1.378(3)
N(5B)-C(9B)	1.311(4)	N(5D)-C(9D)	1.317(4)
Bond	Angle/°	Bond	Angle/°
C(1)-N(1)-C(8)	108.4(2)	C(1C)-N(1C)-C(8C)	108.8(2)
C(10)-N(2)-C(9)	109.0(2)	C(9C)-N(2C)-C(10C)	108.6(2)
C(10)-N(2)-N(3)	124.8(2)	C(9C)-N(2C)-N(3C)	126.4(2)
C(9)-N(2)-N(3)	126.2(2)	C(10C)-N(2C)-N(3C)	124.9(2)
C(10)-N(4)-N(5)	113.2(2)	C(10C)-N(4C)-N(5C)	113.1(2)
C(9)-N(5)-N(4)	104.5(2)	C(9C)-N(5C)-N(4C)	104.1(2)
N(1)-C(1)-C(2)	129.4(3)	N(1C)-C(1C)-C(2C)	129.8(3)
N(1)-C(1)-C(6)	107.9(2)	N(1C)-C(1C)-C(6C)	107.7(2)
C(1B)-N(1B)-C(8B)	108.4(2)	C(1D)-N(1D)-C(8D)	108.7(2)
C(10B)-N(2B)-C(9B)	108.2(2)	C(10D)-N(2D)-C(9D)	109.1(2)
C(10B)-N(2B)-N(3B)	125.5(2)	C(10D)-N(2D)-N(3D)	125.4(2)
C(9B)-N(2B)-N(3B)	126.3(2)	C(9D)-N(2D)-N(3D)	125.4(2)
C(10B)-N(4B)-N(5B)	113.2(2)	C(10D)-N(4D)-N(5D)	113.1(2)
C(9B)-N(5B)-N(4B)	104.5(2)	C(9D)-N(5D)-N(4D)	104.2(2)
N(1B)-C(1B)-C(2B)	129.5(3)	N(1D)-C(1D)-C(2D)	129.9(3)
N(1B)-C(1B)-C(6B)	108.2(2)	N(1D)-C(1D)-C(6D)	107.8(2)

The molecular packing of **1** is presented in Figure 6 while the hydrogen bond parameters are depicted in Table 5. There are a large number of polar N-H ... N and N-H ... S hydrogen bonds which connect the molecules of compound **1** via complicated sets of hydrogen bonding interactions. The donor-acceptor distances for the N-H ... N hydrogen bonds are in the range of 3.010(4) Å (N3-H3B ... N5) to 3.157(4) Å (N1C-H1C ... N3C). On the other hand, the respective values for the N-H ... S hydrogen bonds range from 3.306(3) Å (N4B-H4B ... S1D) to 3.576(3) Å (N1B-H1B ... S1C).

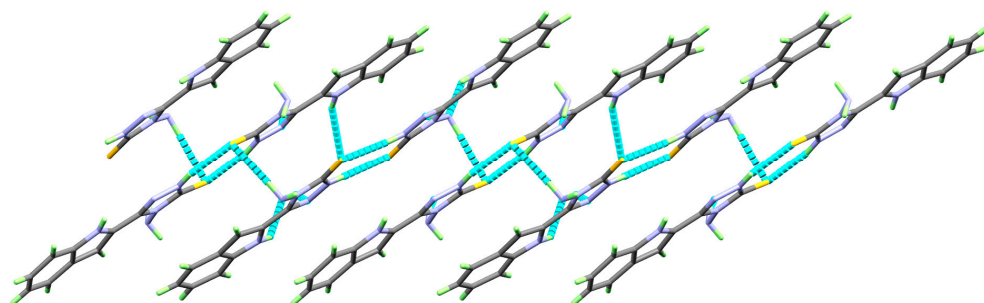
**Figure 6.** The molecular packing scheme for **1**.

Table 5. Hydrogen bonds for **1** [\AA and $^\circ$].

D-H ... A	d(D-H)	d(H ... A)	d(D ... A)	$\angle(\text{DHA})$	Symm. Code
N1-H1 ... N3	0.88(4)	2.30(4)	3.122(4)	154(3)	$-1 + x, y, z$
N1B-H1B ... S1C	0.83(4)	2.82(4)	3.577(3)	154(3)	$1 + x, y, z$
N1C-H1C ... N3C	0.85(4)	2.43(4)	3.157(3)	144(3)	$1 + x, y, z$
N3-H3A ... S1D	0.93(4)	2.58(4)	3.455(3)	157(3)	$x, y, -1 + z$
N3-H3B ... N5	0.93(4)	2.28(4)	3.011(3)	136(3)	$1 + x, y, z$
N4-H4 ... S1C	0.93(4)	2.42(4)	3.342(2)	171(3)	$x, y, -1 + z$
N4B-H4B ... S1D	0.88(4)	2.43(4)	3.306(3)	171(3)	$x, y, -1 + z$
N4C-H4C ... S1	0.78(4)	2.54(4)	3.322(3)	178(4)	$x, y, 1 + z$
N4D-H4D ... S1B	0.82(4)	2.54(4)	3.352(3)	170(3)	$x, y, 1 + z$
N3C-H3CA ... S1B	0.97(4)	2.53(4)	3.440(3)	157(3)	
N3C-H3CB ... N5C	0.80(4)	2.42(4)	3.076(3)	140(3)	$-1 + x, y, z$
N3B-H3BA ... N5B	0.89(4)	2.37(4)	3.113(4)	141(4)	$-1 + x, y, z$
N3D-H3DB ... N5D	0.88(4)	2.30(4)	3.044(3)	143(3)	

3.2. Hirshfeld Surface (HS) Analysis

Analysis of the possible non-covalent interactions using Hirshfeld calculations in crystalline materials gave a complete picture of the different forces which stabilize the crystal structure. All possible non-covalent interactions present in the crystal structure of **3** along with their net percentages are presented graphically in Figure 7 (blue bars). In the same figure, the percentage contributions of the interaction of all the atoms present inside the HS with an atom outside the HS (brown bars) as well as the percentage contributions of the interaction of an atom present inside the HS with all the atoms present in the surrounding area of the HS (green bars) are presented. The H ... H (39.6%), H ... C (22.0%), N ... H (12.8%) and Br ... H (13.2%) contacts are the most dominant in the crystal structure of this compound. Other minor contacts such as the S ... H (3.3%), C ... N (3.0%), Br ... S (2.8%) and Br ... C (0.3%) are detected in the crystal structure of **3**.

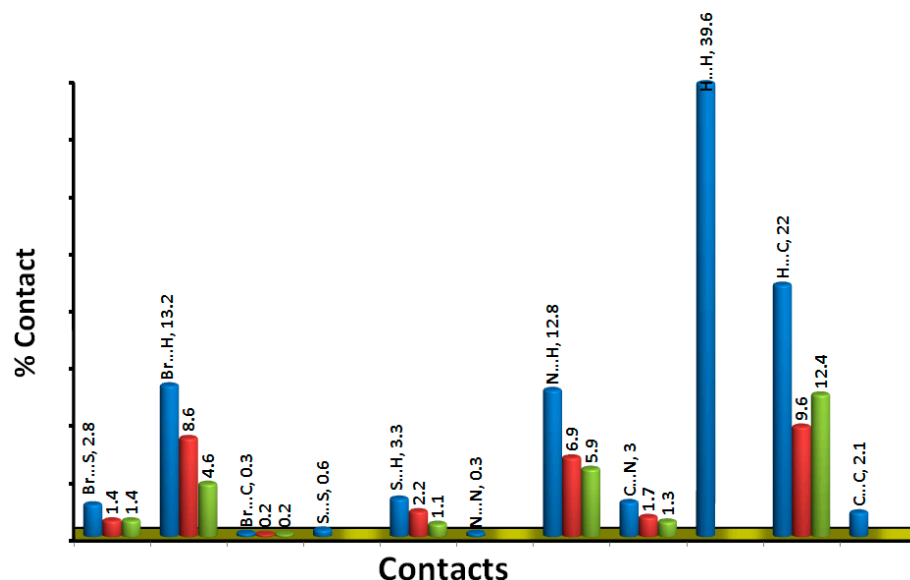


Figure 7. Intermolecular contacts and their percentages in **3**. Color codes: blue (all interactions); brown (in/out) and green (out/in).

The different mapped surfaces resulting from the Hirshfeld calculations are presented in Figure 8. In the d_{norm} map, the red regions are related to the C ... C, C ... H, Br ... H, N ... H, S ... S and Br ... C contacts. The short intermolecular interactions are listed in Table 6. The C3 ... C6 (2.367 \AA), C3 ... H13C (2.548 \AA), Br1 ... H1A (3.196 \AA), N2 ... H3 (1.849 \AA), and Br1 ... C1 (3.470 \AA) are the shortest distance non-covalent interactions.

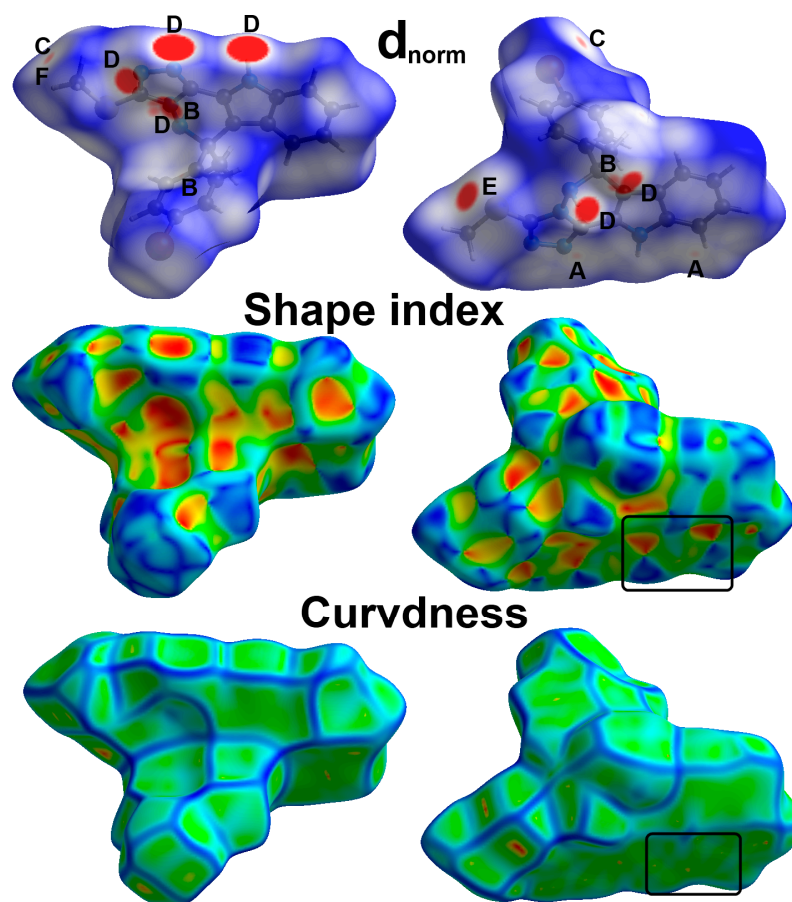


Figure 8. Hirshfeld surfaces of **3** showing the most important interactions (A) C ... C, (B) C ... H, (C) Br ... H, (D) N ... H, (E) S ... S and (F) Br ... C.

Table 6. Short contacts in **3**.

Contact	Distance	Contact	Distance
C3 ... C6	2.367	Br1 ... H1B	3.215
C16 ... H13B	2.764	N2 ... H3	1.849
C3 ... H13C	2.548	N1 ... H4	2.311
C2 ... H13C	2.725	N1 ... H3	2.585
Br1 ... C1	3.47	N2 ... H13C	2.448
Br1 ... H1A	3.196	N1 ... H13C	2.577
S1 ... S1	3.286		

The shape index and curvedness of surfaces are essential to confirm the presence of π - π stacking interactions. It is clear that the red/blue triangles in the shape index and flat green area in curvedness indicated the presence of π - π stacking interactions (Figure 8). In accord with this observation, the percentage of C ... C contacts is 2.1%. In addition, the decomposed fingerprint (FP) plots of all short contacts are shown in Figure 9. Without doubt, the sharp spikes in the FP plots of the majority of these contacts confirmed their importance where all have shorter distances than the vdWs radii sum of the interacting atoms (Table 6).

For **1**, there are four molecules of this compound in the asymmetric formula. In this case, the d_{norm} map of each molecule was calculated separately and the possible intermolecular interactions are analyzed and presented in Figures 10 and 11, respectively. The four molecules in the asymmetric unit have common types of non-covalent interactions but their percentages are slightly different in the four units.

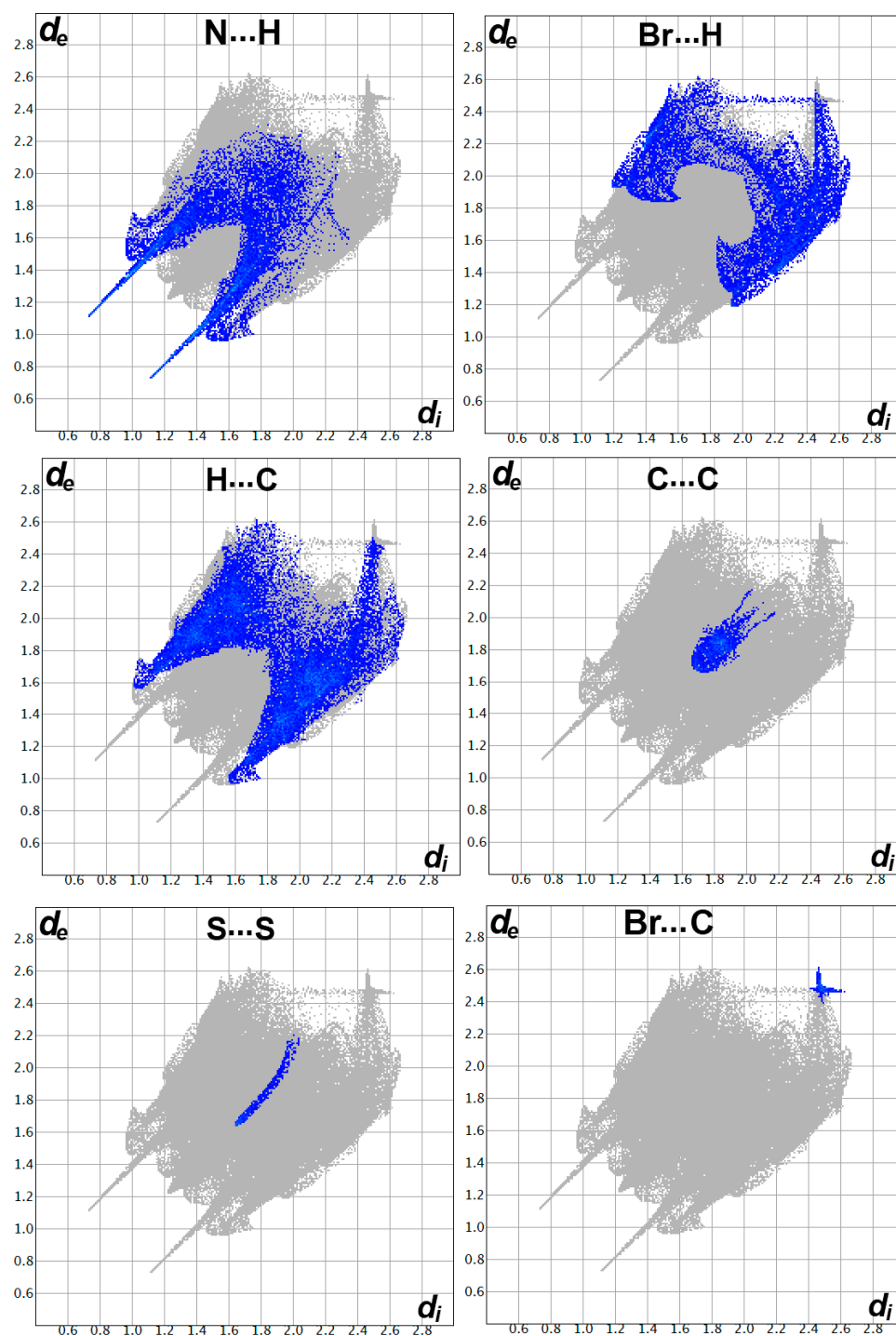


Figure 9. Decomposed fingerprint plots for the short contacts in **3**.

For **1**, there are four molecules of this compound in the asymmetric formula. In this case, the d_{norm} map of each molecule was calculated separately and the possible intermolecular interactions are analyzed and presented in Figures 10 and 11, respectively. The four molecules in the asymmetric unit have common types of non-covalent interactions but their percentages are slightly different in the four units.

Careful inspection of the d_{norm} maps of the four units indicated the presence of a number of short non-covalent interactions which are generally shorter than the vdWs radii sum of the two atoms sharing these contacts (Table 7). These interactions which are considered important in the molecular packing of **1** are seen in the d_{norm} map as red

spots. In this structure, the C...H, N...H, S...H, S...S, and C...C contacts are the most important.

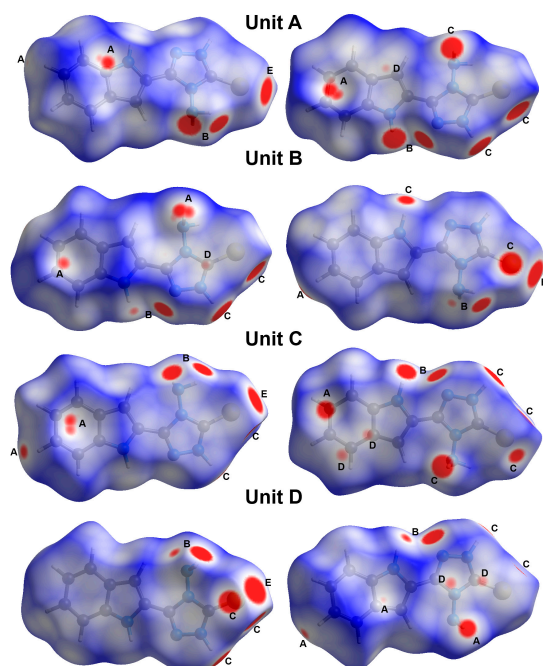


Figure 10. Hirshfeld d_{norm} surfaces for the four molecules in the asymmetric formula of **1** showing the most important interactions (A) C...H, (B) N...H, (C) S...H, (D) C...C and (E) S...S.

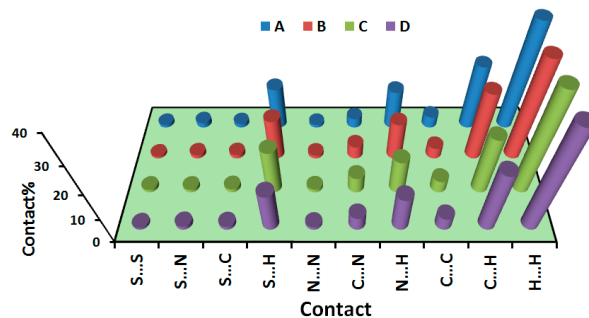


Figure 11. Distribution of all intermolecular contacts in the four molecules of **1** in the asymmetric formula.

Table 7. All possible non-covalent interactions and their percentages in **1**.

Contact	Distance	Contact	Distance
C1...H3C	2.619	N5...H3B	2.214
C2...H3C	2.743	N3...H1	2.193
C6D...H3	2.754	N5B...H3BA	2.275
C2...H3BB	2.67	N3B...H1B	2.554
C3...H3BB	2.614	N3C...H1C	2.301
C4...H3BB	2.754	N5C...H3CB	2.263
C3B...H4DA	2.671	N5D...H3DB	2.197
C5C...H4BA	2.787	N3D...H1D	2.51
C4C...H4BA	2.661	S1...H4C	2.314
C3C...H4BA	2.692	S1C...H4	2.341
C4C...H3DA	2.759	S1D...H3A	2.505
C3C...H3DA	2.526	S1B...H4D	2.354
C1...H3C	2.619	S1D...H4B	2.309
H3C...C2	2.743	S1C...H1B	2.656
S1...S1C	3.167	C7...C10B	3.354
S1B...S1D	3.137	C5...C9B	3.39

Decomposition of the fingerprint plots gave accurate percentages of all possible contacts in the crystal structure. It was found that, the H...H, C...H, N...H and S...H contacts are the most dominant in all units. Their percentages range from 34.9 to 37.4, 20.5 to 24.0, 12.2 to 13.6 and 14.0 to 15.8%, respectively (Table 8). In addition, the sharp spikes in the decomposed fingerprint plots of these contacts indicate short distance interactions and are considered strong (Figure 12).

Table 8. Percentages of all contacts in 1^a.

Contact	A	B	C	D
S...S	1.1	0.8	1.1	0.8
S...N	1.8 (1.3,0.5)	1.3 (0.5,0.8)	1.1 (0.6,0.5)	1.4 (0.6,0.8)
S...C	1.4 (0.7,0.7)	1.4 (0.7,0.7)	1.3 (0.3,0.9)	1.3 (1.0,0.3)
S...H	14.6 (9.0,5.7)	14.5 (9.6,4.9)	15.8 (10.0,5.8)	14.0 (9.4,4.7)
N...N	1.1	1.2	1.2	1.1
C...N	3.4 (1.4,2.0)	4.6 (2.7,1.9)	5.8 (2.7,3.1)	5.0 (2.8,2.2)
N...H	13.6 (7.8,5.7)	13.3 (7.8,5.5)	12.2 (6.9,5.3)	12.6 (6.9,5.7)
C...C	4.1	4.0	4.5	4.6
C...H	22.4 (14.0,8.3)	24.0 (12.8,11.3)	20.5 (12.2,8.3)	21.8 (12.5,9.3)
H...H	36.5	34.9	36.5	37.4

^a Values inside parentheses are the percentage contributions of the interaction of all the atoms present inside the HS with an atom outside the HS, and the percentage contributions of the interaction of an atom present inside the HS with all the atoms present in the surrounding area of the HS, respectively.

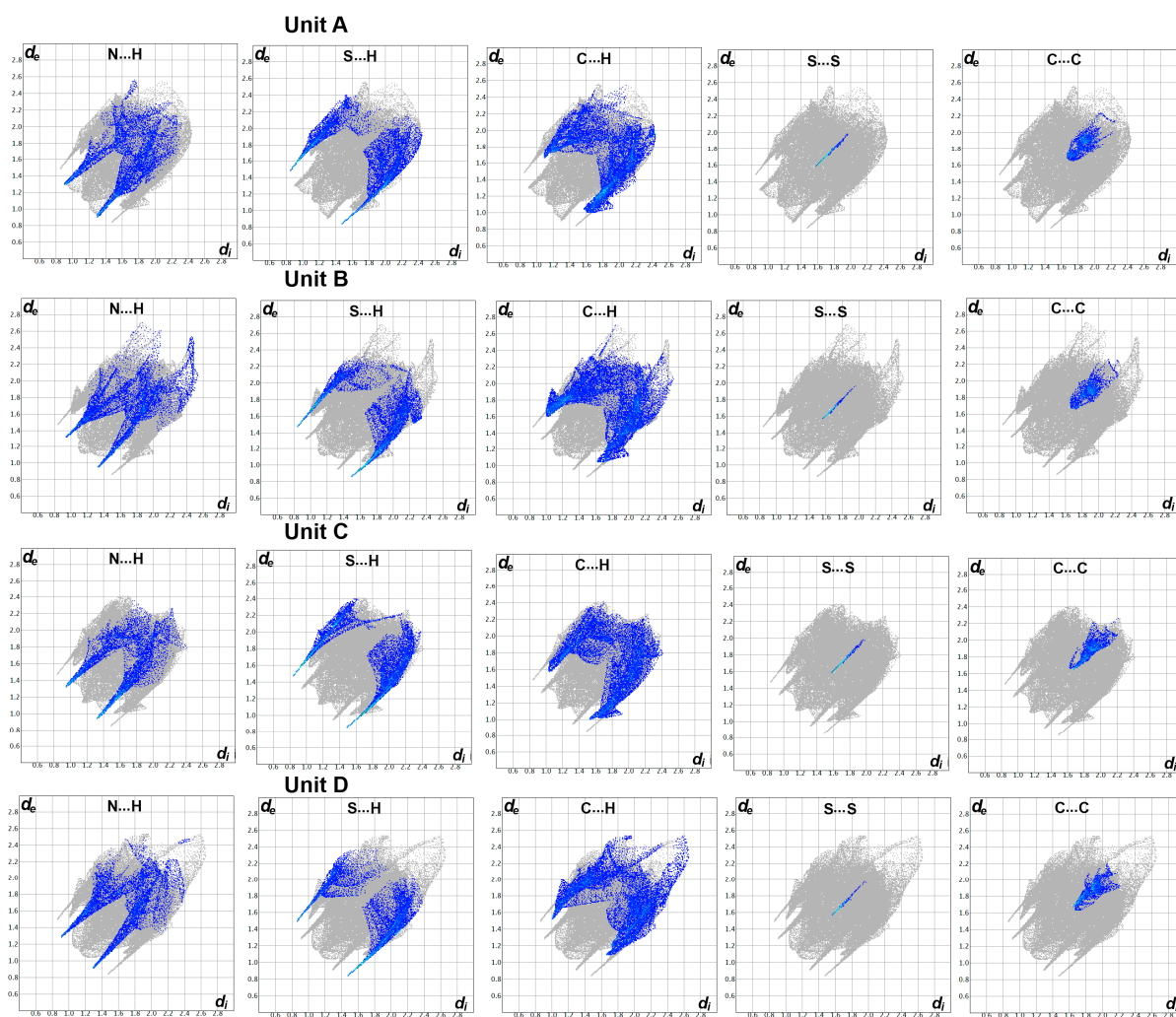


Figure 12. Decomposed fingerprint plots for the short contacts in 1.

4. Conclusions

Compound **1**, 4-Amino-5-indolyl-1,2,4-triazole-3-thione, reacted with 4'-bromoacetophenone **2** in methanol and concentrated HCl to give the target compound 1,2,4-triazolo pyridazino[4,5-*b*]indole **3** in good yield. Crystals suitable for X-ray single crystal analysis were obtained by recrystallization from methanol. The structure of both compounds was analyzed using Hirshfeld calculations based on their accurately determined X-ray structures. While **3** crystallized in the triclinic crystal system and *P*-1 space, compound **1** crystallized in the less symmetric monoclinic crystal system and *P*2₁ space group. In the former, the triazole and indole rings are twisted from each other by 12.64°, while the corresponding values in **1** are in the range 4.94–7.22°. Hirshfeld analysis indicated the significance of the C...C, C...H, N...H and S...S contacts in both compounds. Additionally, some short Br...H interactions were detected in **3**. In both systems, the shape index and curvedness maps confirmed the presence of π - π stacking interactions. Quantitative determinations of the non-covalent interactions that occurred in both crystals indicated that the H...H (35.3%), H...C (22.5%), N...H (15.4%) and Br...H (13.2%) contacts are the most dominant in **3** while the H...H (34.9 to 37.4%), C...H (20.5 to 24.0%), N...H (12.2 to 13.6%) and S...H (14.0 to 15.8%) contacts are the most abundant in **1**.

Supplementary Materials: The following supporting information can be downloaded at: <https://www.mdpi.com/article/10.3390/cryst13071036/s1>, the CIF data of compounds **3** and **1**. were provided as CCDC_2266558.cif and CCDC_2266559.cif. Figure S1: ¹HNMR of compound **1**; Figure S2: ¹³CNMR of compound **1**; Figure S3: ¹HNMR of compound **3**; Figure S4: ¹³CNMR of compound **3**.

Author Contributions: Conceptualization, A.T.A.B., M.S. and A.B.; methodology, M.S. and A.T.A.B.; software, S.M.S. and M.H.; validation, E.H.E., A.T.A.B. and A.B.; formal analysis, M.S. and A.T.A.B.; investigation, A.T.A.B., S.M.S. and A.B.; resources, A.T.A.B. and A.B.; data curation, S.M.S. and M.H.; writing—original draft preparation, A.T.A.B.; writing—review and editing, A.T.A.B., A.B., S.M.S., E.H.E., M.H. and M.S.; visualization, A.T.A.B. and A.B.; supervision, A.T.A.B.; project administration, A.B.; funding acquisition, A.B. All authors have read and agreed to the published version of the manuscript.

Funding: The authors would like to extend their sincere appreciation to the Researchers Supporting Project (RSP2023R64), King Saud University, Riyadh, Saudi Arabia.

Data Availability Statement: Not applicable.

Acknowledgments: The authors would like to extend their sincere appreciation to the Researchers Supporting Project (RSP2023R64), King Saud University, Riyadh, Saudi Arabia.

Conflicts of Interest: The authors declare no conflict of interest.

References

1. Henary, M.; Kananda, C.; Rotolo, L.; Savino, B.; Owens, E.A.; Cravotto, G. Benefits and applications of microwave-assisted synthesis of nitrogen containing heterocycles in medicinal chemistry. *RSC Adv.* **2020**, *10*, 14170–14197. [[CrossRef](#)] [[PubMed](#)]
2. Kerru, N.; Gummidi, L.; Maddila, S.; Gangu, K.K.; Jonnalagadda, S.B. A Review on Recent Advances in Nitrogen-Containing Molecules and Their Biological Applications. *Molecules* **2020**, *25*, 1909. [[CrossRef](#)] [[PubMed](#)]
3. Bruel, A.; Bénétteau, R.; Chabanne, M.; Lozach, O.; Le Guevel, R.; Ravache, M.; Bénédetti, H.; Meijer, L.; Logé, C.; Robert, J.M. Synthesis of new pyridazino [4, 5-*b*] indol-4-ones and pyridazin-3 (2H)-one analogs as DYRK1A inhibitors. *Bioorg. Med. Chem. Lett.* **2014**, *24*, 5037. [[CrossRef](#)] [[PubMed](#)]
4. Bruel, A.; Logé, C.; de Tauzia, M.-L.; Ravache, M.; Le Guevel, R.; Guillouzo, C.; Lohier, J.-F.; Santos, J.S.-D.O.; Lozach, O.; Meijer, L.; et al. Synthesis and biological evaluation of new 5-benzylated 4-oxo-3,4-dihydro-5H-pyridazino[4,5-*b*]indoles as PI3K α inhibitors. *Eur. J. Med. Chem.* **2012**, *57*, 225–233. [[CrossRef](#)]
5. Avan, I.; Güven, A.; Güven, K. Synthesis and antimicrobial investigation of some 5H-pyridazino[4,5-*b*]indoles. *Turk. J. Chem.* **2013**, *37*, 271–291. [[CrossRef](#)]
6. El-Gendy, A.A.; Said, M.M.; Ghareb, N.; Mostafa, Y.M.; El-Ashry, E.S.H. Synthesis and Biological Activity of Functionalized Indole-2-carboxylates, Triazino- and Pyridazino-indoles. *Arch. Pharm.* **2008**, *341*, 294. [[CrossRef](#)]
7. El-Gendy, A.A.; El-Banna, H.A. Synthesis and antihypertensive activity of certain Mannich Bases of 2-ethoxycarbonylindoles and 5H-pyridazino[4,5-*b*]indoles. *Arch. Pharmacol. Res.* **2001**, *24*, 21–26. [[CrossRef](#)]

8. Monge, A.; Parrado, P.; Font, M.; Fernandez-Alvarez, E. Selective thromboxane synthetase inhibitors and antihypertensive agents. New derivatives of 4-hydrazino-5H-pyridazino [4, 5-b] indole, 4-hydrazinotriazino [4, 5-a] indole, and related compounds. *J. Med. Chem.* **1987**, *30*, 1029. [[CrossRef](#)]
9. Font, M.; Monge, A.; Cuartero, A.; Elorriaga, A.; Martínez-Irujo, J.; Alberdi, E.; Santiago, E.; Prieto, I.; Lasarte, J.; Sarobe, P.; et al. Indoles and pyridazino[4,5-b]indoles as nonnucleoside analog inhibitors of HIV-1 reverse transcriptase. *Eur. J. Med. Chem.* **1995**, *30*, 963–971. [[CrossRef](#)]
10. Monge, A.; Aldana, I.; Alvarez, T.; Font, M.; Santiago, E.; Latre, J.A.; Bermejillo, M.J.; Lopez-Unzu, M.J.; Fernandez-Alvarez, E. New 5H-pyridazino[4,5-b]indole derivatives. Synthesis and studies as inhibitors of blood platelet aggregation and inotropics. *J. Med. Chem.* **1991**, *34*, 3023–3029. [[CrossRef](#)]
11. Sravanthi, T.V.; Manju, S.L. Indoles—A Promising Scaffold for Drug Development. *Eur. J. Pharm. Sci.* **2016**, *91*, 1–10. [[CrossRef](#)]
12. Chen, J.; Dong, X.; Liu, T.; Lou, J.; Jiang, C.; Huang, W.; He, Q.; Yang, B.; Hu, Y. Design, synthesis, and quantitative structure–activity relationship of cytotoxic γ -carboline derivatives. *Bioorg. Med. Chem.* **2009**, *17*, 3324. [[CrossRef](#)]
13. Vin, V.; Leducq, N.; Bono, F.; Herbert, J. Binding characteristics of SSR180575, a potent and selective peripheral benzodiazepine ligand. *Biochem. Biophys. Res. Commun.* **2003**, *310*, 785–790. [[CrossRef](#)]
14. Papadopoulos, V.; Baraldi, M.; Guilarte, T.R.; Knudsen, T.B.; Lacapère, J.-J.; Lindemann, P.; Norenberg, M.D.; Nutt, D.; Weizman, A.; Zhang, M.-R.; et al. Translocator protein (18kDa): New nomenclature for the peripheral-type benzodiazepine receptor based on its structure and molecular function. *Trends Pharmacol. Sci.* **2006**, *27*, 402–409. [[CrossRef](#)]
15. Zhou, G.F.; Qian, W.; Li, F.; Yang, R.H.; Wang, N.; Zheng, C.B.; Li, C.Y.; Gu, X.R.; Yang, L.M.; Liu, J.; et al. Discovery of ZFD-10 of a pyridazino [4, 5-b] indol-4 (5H)-one derivative as an anti-ZIKV agent and a ZIKV NS5 RdRp inhibitor. *Antivir. Res.* **2023**, *214*, 105607. [[CrossRef](#)]
16. Sarhan, A.A.; Boraie, A.T.; Barakat, A.; Nafie, M.S. Discovery of hydrazide-based pyridazino [4, 5-b] indole scaffold as a new phosphoinositide 3-kinase (PI3K) inhibitor for breast cancer therapy. *RSC Adv.* **2020**, *10*, 19534–19541. [[CrossRef](#)]
17. Wubben, T.J.; Chaudhury, S.; Watch, B.T.; Stuckey, J.A.; Weh, E.; Fernando, R.; Goswami, M.; Pawar, M.; Rech, J.C.; Besirli, C.G. Development of Novel Small-Molecule Activators of Pyruvate Kinase Muscle Isozyme 2, PKM2, to Reduce Photoreceptor Apoptosis. *Pharmaceuticals* **2023**, *16*, 705. [[CrossRef](#)]
18. Salama, E.E.; Althobaiti, I.O.; Haukka, M.; Boraie, A.T.A. Synthesis, X-ray Single-Crystal Analysis, and Anticancer Activity Evaluation of New Alkylsulfanyl-Pyridazino[4,5-b]indole Compounds as Multitarget Inhibitors of EGFR and Its Downstream PI3K-AKT Pathway. *Crystals* **2022**, *12*, 353. [[CrossRef](#)]
19. Kochanowska-Karamyan, A.J.; Hamann, M.T. Marine Indole Alkaloids: Potential New Drug Leads for the Control of Depression and Anxiety. *Chem. Rev.* **2010**, *110*, 4489–4497. [[CrossRef](#)]
20. Festa, A.A.; Voskressensky, L.G.; Van der Eycken, E.V. Visible light-mediated chemistry of indoles and related heterocycles. *Chem. Soc. Rev.* **2019**, *48*, 4401–4423. [[CrossRef](#)]
21. Chadha, N.; Silakari, O. Indoles as therapeutics of interest in medicinal chemistry: Bird’s eye view. *Eur. J. Med. Chem.* **2017**, *134*, 159–184. [[CrossRef](#)] [[PubMed](#)]
22. Kaushik, N.K.; Kaushik, N.; Attri, P.; Kumar, N.; Kim, C.H.; Verma, A.K.; Choi, E.H. Biomedical Importance of Indoles. *Molecules* **2013**, *18*, 6620–6662. [[CrossRef](#)] [[PubMed](#)]
23. Wermuth, C.G. Are Pyridazines Privileged Structures? *Med. Chem. Commun.* **2011**, *2*, 935–941. [[CrossRef](#)]
24. Volonterio, A.; Moisan, L.; Rebek, J. Synthesis of Pyridazine-Based Scaffolds as α -Helix Mimetics. *Org. Lett.* **2007**, *9*, 3733–3736. [[CrossRef](#)]
25. Butnariu, R.M.; Mangalagiu, I.I. New pyridazine derivatives: Synthesis, chemistry and biological activity. *Bioorg. Med. Chem.* **2009**, *17*, 2823–2829. [[CrossRef](#)]
26. Campagna, F.; Palluotto, F.; Mascia, M.P.; Maciocco, E.; Marra, C.; Carotti, A.; Carrieri, A. Synthesis and biological evaluation of pyridazino[4,3-b]indoles and indeno[1,2-c]pyridazines as new ligands of central and peripheral benzodiazepine receptors. *Il Farm.* **2003**, *58*, 129–140. [[CrossRef](#)]
27. Panathur, N.; Gokhale, N.; Dalimba, U.; Koushik, P.V.; Yogeewari, P.; Sriram, D. Synthesis of novel 5-[(1,2,3-triazol-4-yl)methyl]-1-methyl-3H-pyridazino[4,5-b]indol-4-one derivatives by click reaction and exploration of their anticancer activity. *Med. Chem. Res.* **2016**, *25*, 135–148. [[CrossRef](#)]
28. Sircar, I.; Steffen, R.P.; Bobowski, G.; Burke, S.F.; Newton, R.S.; Weishaar, R.E.; Bristol, J.A.; Evans, D.B. Cardiotonic agents. 9. Synthesis and biological evaluation of a series of (E)-4, 5-dihydro-6-[2-[4-(1H-imidazol-1-yl) phenyl] ethenyl]-3 (2H)-pyridazinones: A novel class of compounds with positive inotropic, antithrombotic, and vasodilatory activities for the treatment of congestive heart failure. *J. Med. Chem.* **1989**, *32*, 342.
29. Bare, T.M.; Resch, J.F.; Jackson, P.F. EP 512817, 1992. *Chem. Abstr.* **1993**, *118*, 101975.
30. Nantka-Namirski, P.; Ozdowska, Z. 2-Carbethoxyindole derivatives. I. Synthesis of 8-alkoxy- and 8,9-benzo-3H-pyridazino(4,5-b) indol-4-ones. *Acta Pol. Pharm.* **1972**, *29*, 9–15.
31. Ilardi, E.A.; Vitaku, E.; Njardarson, J.T. Data-Mining for Sulfur and Fluorine: An Evaluation of Pharmaceuticals To Reveal Opportunities for Drug Design and Discovery. *J. Med. Chem.* **2014**, *57*, 2832–2842. [[CrossRef](#)]
32. Feng, M.; Tang, B.; Liang, S.H.; Jiang, X. Sulfur Containing Scaffolds in Drugs: Synthesis and Application in Medicinal Chemistry. *Curr. Top. Med. Chem.* **2016**, *16*, 1200–1216. [[CrossRef](#)]

33. Boraie, A.T.A. A new direct synthetic access to 4-Amino-2-N-(glycosyl/propyl)-1,2,4-triazole-3-thiones via hydrazinolysis of 3-N-((Acylated glycosyl)/allyl)-1,3,4-oxadiazole-2-thiones. *Arkivoc* **2016**, *iii*, 71–81. [[CrossRef](#)]
34. Otwinowski, Z.; Minor, W. Processing of X-ray Diffraction Data Collected in Oscillation Mode. *Methods Enzymol.* **1997**, *276*, 307–326. [[CrossRef](#)]
35. Rigaku Oxford Diffraction. *CrysAlisPro*; Agilent Technologies Inc.: Oxfordshire, UK, 2020.
36. Sheldrick, G.M. SHELXT—Integrated space-group and crystal-structure determination. *Acta Cryst.* **2015**, *A71*, 3–8. [[CrossRef](#)]
37. Sheldrick, G.M. *SADABS—Bruker Nonius Scaling and Absorption Correction*; Bruker AXS, Inc.: Madison, WI, USA, 2012.
38. Sheldrick, G.M. Crystal structure refinement with SHELXL. *Acta Cryst.* **2015**, *C71*, 3–8. [[CrossRef](#)]
39. Hübschle, C.B.; Sheldrick, G.M.; Dittrich, B. ShelXle: A Qt graphical user interface for SHELXL. *J. Appl. Cryst.* **2011**, *44*, 1281–1284. [[CrossRef](#)]
40. Turner, M.J.; McKinnon, J.J.; Wolff, S.K.; Grimwood, D.J.; Spackman, P.R.; Jayatilaka, D.; Spackman, M.A. Crystal Explorer17, University of Western Australia. 2017. Available online: <https://crystalexplorer.net/> (accessed on 30 July 2020).

Disclaimer/Publisher’s Note: The statements, opinions and data contained in all publications are solely those of the individual author(s) and contributor(s) and not of MDPI and/or the editor(s). MDPI and/or the editor(s) disclaim responsibility for any injury to people or property resulting from any ideas, methods, instructions or products referred to in the content.